

Structural investigation of $\text{Pb}_y(\text{Zr}_{0.57}\text{Ti}_{0.43})_{2-y}\text{O}_3$ films deposited on Pt(001)/MgO(001) substrates by rf sputtering

Toshiyuki Matsunaga, Teppei Hosokawa, and Yukihiro Umetani

Characterization Technology Group, Matsushita Technoresearch, Inc., 3-1-1 Yagumo-Nakamachi, Moriguchi, Osaka 570-8501, Japan

Ryouichi Takayama

Color Printing Products & Technology Development Center, Matsushita Electric Industrial Co., Ltd., 3-1-1 Yagumo-Nakamachi, Moriguchi, Osaka 570-8501, Japan

Isaku Kanno

Department of Mechanical Engineering, Graduate School of Engineering, Kyoto University, Yoshida-Honmachi, Sakyo-ku, Kyoto 606-8501, Japan

(Received 8 February 2002; published 6 August 2002)

We performed structural studies on PZT thin films, $\text{Pb}_y(\text{Zr}_{0.57}\text{Ti}_{0.43})_{2-y}\text{O}_3$; $y=0.97, 1.07, 1.15$. The thin films were deposited on Pt (001)/MgO (001) substrates by rf-magnetron sputtering. Every film grew epitaxially in a tetragonal phase with the “cube on cube” relationship to the substrate, and contained no other crystalline phases, such as PbO or pyrochlore. It is known that PZT bulk ceramic with Zr/Ti of about 57/43, the composition of which is on the Zr-rich side of the morphotropic phase boundary (MPB), has a rhombohedral structure at room temperature. These PZT films, however, had tetragonal perovskite structures (space group: $P4mm$). The Pb atoms mainly occupy the A ($1a$) site, and the Zr and Ti atoms occupy the B ($1b$) site at random. When y is less than unity in $\text{Pb}_y(\text{Zr}_{0.57}\text{Ti}_{0.43})_{2-y}\text{O}_3$, the excess Zr/Ti tends to enter the Pb (A) sites and randomly occupy the sites together with Pb; and when y is more than unity, the excess Pb tends to mix with the Zr and Ti at Zr/Ti (B) sites. In all these films, the atomic positions of Zr/Ti, O(1), and O(2) shift mutually along the c axis in the tetragonal structure. With increasing y , c/a approaches unity and the crystal structure shifts toward the rhombohedral phase, especially in the O(2) atomic position, where a large shift was observed. The PZT thin films were grown under the restraint of a Pt (001) square lattice, and under isotropic compressive plane stress. These are the major reasons that the film crystallizes into tetragonal perovskite and polarizes spontaneously in the c -axis direction perpendicular to the substrate surface.

DOI: 10.1103/PhysRevB.66.064102

PACS number(s): 61.10.Nz

I. INTRODUCTION

$\text{Pb}(\text{Zr},\text{Ti})\text{O}_3$, abbreviated as PZT, has superior ferroelectric, pyroelectric, and piezoelectric characteristics and is widely used in various functional device applications. PZT ceramics show their maximum dielectric and piezoelectric properties, especially in the composition region around the MPB (morphotropic phase boundary). At room temperature, the crystal structure is tetragonal on the Ti-rich side of the MPB and rhombohedral on the Zr-rich side (see Fig. 1). When the temperature rises, a center of symmetry appears in both structures, the structure is transformed into a cubic phase, and it loses its spontaneous polarization. However, it has been found recently that the tetragonal phase is transformed into a low-temperature monoclinic phase in a narrow composition region near MPB.² Most previous studies on these crystal structures have used bulk materials, i.e., ceramics. Active research and development, however, is being carried out into the potential use of thin-film PZT materials in nonvolatile memory or microelectromechanical systems (MEMS).

These thin films exhibit unique structural characteristics that differ from those of their bulk materials, since the films generally grow under the constraint of substrates, often accumulating considerable stress. Furthermore, deposition via plasma such as rf sputtering uses activated sputtered particles

with high kinetic energy, which lead to nonthermal equilibrium in the crystallization process of the PZT different from the growth on bulk materials. Probably for these reasons, the dielectric properties of perovskitetype thin films are different from those of their equivalent bulk materials, as has been reported in Ref. 3. Although the electrical properties of PZT

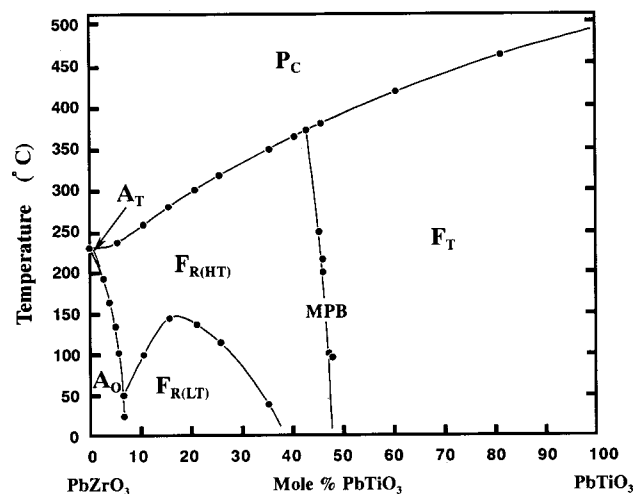


FIG. 1. The phase diagram of the lead zirconate titanate (PZT) system according to Jaffe *et al.* (Ref. 1).

TABLE I. Growth conditions for the PZT thin films.

Target	$[\text{Pb}(\text{Zr}_{0.57}\text{Ti}_{0.43})\text{O}_3]_y + [\text{PbO}]_{1-y}$ $y = 0.7, 0.8, 0.9$
Substrate	Pt (001)/MgO (001)
Sub. temperature	500–600 °C
rf power	500 W/6" ϕ
Growth rate	$\sim 1.0 \mu\text{m/hr}$
Film thickness	$\sim 3 \mu\text{m}$

are presumed to be closely related to its crystal structure, up to now little has been known about the detailed crystal structures of the films. This is because deposited film specimens are usually too oriented and too thin, giving insufficient x-ray-diffraction intensity data to allow precise structural analyses.

We have solved this problem by peeling the thin film off the substrate, powdering it, and analyzing it using synchrotron radiation and a large-diameter Debye-Scherrer camera with an imaging plate. The Debye-Scherrer camera allows simultaneous collection of multiple diffraction lines. In contrast to the line spectrum generated by an x-ray tube, the synchrotron radiation spectrum is smooth over a wide range of energies. This makes it possible to choose the wavelength best suited to the experimental problem in question. Moreover, synchrotron radiation facilities generate intense x rays, making it possible to collect precise x-ray-diffraction data within a reasonably short time even if there is only a small quantity of the specimen.

In this paper, the crystal structures of epitaxial thin films with different Pb/(Zr+Ti) ratios ($y = 0.97, 1.07, 1.15$) in $\text{Pb}_y(\text{Zr}_{0.57}\text{Ti}_{0.43})_{2-y}\text{O}_3$ were analyzed in detail employing the powder x-ray-diffraction method after having examined the crystallographic characteristics of the films employing a lab-based high-resolution x-ray diffractometer. We will describe the results of the structural analyses, and the influence that substrates have on the crystal structures.

II. EXPERIMENT

Three types of PZT thin films with different Pb/(Zr + Ti) ratios were fabricated on Pt (001) (with a thickness of about $0.1 \mu\text{m}$) deposited MgO (001) substrates using the rf-magnetron sputtering method. The thickness of the films was about $3 \mu\text{m}$. The sputtering conditions are listed in Table I. Excess PbO (from 10% to 30%) was added to the $\text{Pb}(\text{Zr}_{0.57}\text{Ti}_{0.43})\text{O}_3$ sputtering targets to alter the Pb/(Zr + Ti) ratio in the deposited films. No polarization by external electric field was conducted. The film composition was ex-

amined using a wavelength dispersive x-ray microanalyzer (JEOL JXA-8900R) individually for Pb, Zr, Ti, and O.

The as-grown PZT thin films were first measured using a high-resolution x-ray diffractometer (Rigaku ATX-G) under the following conditions. X rays (50 kV, 40 mA) generated by a sealed Cu target were made parallel and monochromatic using a Ge (220) double monochromator. The lattice constants were obtained by precisely measuring the four-circle diffraction angles of (110), ($\bar{1}10$), (020), and ($\bar{2}00$) by means of the in-plane diffraction method, and of (001) and (002) by means of the out-of-plane diffraction method.⁴ Several $\omega/2\theta$ scanning diffraction patterns along the c^* axis were then obtained, and reciprocal space maps were made in an area including all (204) reciprocal-lattice points of the MgO substrate, and the Pt and PZT thin films. For the mapping, Ge (220) two bounce was employed as the analyzer crystal.

Synchrotron radiation was next used to investigate the intrinsic crystal structure of the PZT film without substrate restriction. After removing the MgO substrate using a wet process, the PZT/Pt film in sheet form was crushed into powder. The powdered PZT/Pt was then packed into a quartz capillary tube with an internal diameter of 0.2 mm. Both ends of the capillary were open to the air. The diffraction experiments were carried out using the large-diameter Debye-Scherrer camera with an imaging plate on the BL02B2 beam line at the Japan Synchrotron Radiation Research Institute (SPring-8).^{5,6} A precollimator mirror and a double crystal spectrometer were used to ensure that the incident beam used for the diffraction experiments was extremely monochromatic and parallel. The camera radius was 278 mm and the pixel area of the imaging plate was $100 \mu\text{m}^2$, corresponding to an angular resolution of approximately 0.02° . To enable precise structural analysis, it is important for each diffraction peak to be comprised of sufficient data points; the diffraction intensity recorded on the imaging plate was read at a pixel area of $50 \mu\text{m}^2$. To confirm the energy of the radiation used, diffraction in CeO_2 ($a = 5.4111 \text{ \AA}$) powder was recorded under the same conditions. All the diffraction experiments were carried out at room temperature.

III. RESULTS

The compositions of the PZT films labeled P1, P2, and P3 are shown in Table II. The oxygen concentration was measured as just under 60 at.% for every specimen. Consequently, the number of oxygen atoms can be assumed to be exactly three per unit cell. The components of the other three metal elements were allocated according to the results of the

TABLE II. Compositions of the PZT thin films obtained by quantitative analyses using a wavelength dispersive x-ray microanalyzer.

Specimen	Pb (at. %)	Zr (at. %)	Ti (at. %)	O (at. %)	Chemical formula
P1	23.4	9.8	7.5	59.3	$\text{Pb}_{1.15}(\text{Zr}_{0.48}\text{Ti}_{0.37})\text{O}_3$
P2	21.4	10.9	7.8	60.0	$\text{Pb}_{1.07}(\text{Zr}_{0.54}\text{Ti}_{0.39})\text{O}_3$
P3	19.2	11.5	8.9	60.3	$\text{Pb}_{0.97}(\text{Zr}_{0.58}\text{Ti}_{0.45})\text{O}_3$

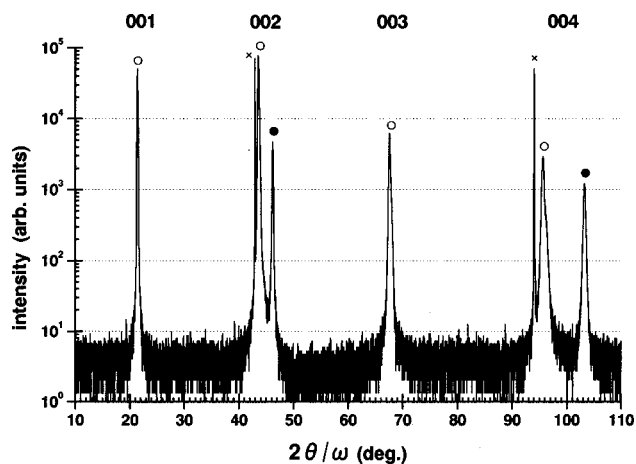


FIG. 2. X-ray double crystal diffraction profile of the PZT/Pt/MgO (P3) heterostructure. The marks, ○, ● and × show the peaks of PZT, Pt, and MgO, respectively.

quantitative analyses. The chemical formulas in the table were derived from the allocations. The $\omega/2\theta$ -wide scan for P3 taken with ATX-G is shown in Fig. 2. It can be seen that both of the Pt and PZT films have been grown with good c -axis orientation. No domains with the other planes parallel to the specimen surface except for (001) are found. The in-plane ϕ scan indicated that the domains are also of uniform orientation parallel to the surface. Almost identical results were also obtained for the other two specimens. The lattice constants of the PZT films are shown in Table III, which reveals that $a=b<c$ and $\alpha=\beta=\gamma=90^\circ$ for every specimen. The unit-cell volume increases with the addition of Pb. Figure 3 shows the (204) reciprocal space map for P3. In the figure, a line was drawn as passing through both the origin and MgO (204) peak position. That of Pt (204) is located close to this line, which means that the Pt film has grown incoherently on the MgO substrate. On the other hand, the peak position of PZT (204) is located in the region of $a<c$ off the line. This also confirms that this PZT film is a tetragonal crystal. Almost identical results were obtained for P1 and P2. The above result shows for every specimen that the a -, b -, and c -axis directions of MgO, Pt, and PZT films are coincident to each other, and that the PZT film is epitaxially grown, almost as a tetragonal single crystal.

The wavelength of the synchrotron radiation used for the x-ray diffraction measurements on the powdered PZT films was 0.4205 \AA . As seen in Fig. 4, the diffraction peaks were detected with a sufficient signal-to-noise ratio up to the vicinity of $2\theta=40^\circ$ ($\sin \theta/\lambda=0.81 \text{ \AA}^{-1}$). All the obtained diffraction patterns for the three specimens are fully explained

TABLE III. Lattice constants for the PZT thin films on Pt/MgO substrates.

Specimen	a (Å)	b (Å)	c (Å)	α (°)	β (°)	γ (°)	V (Å ³)
P1	4.07 ₈	4.07 ₈	4.15 ₂	90.0 ₀	90.0 ₀	90.0 ₁	69.0 ₅
P2	4.06 ₆	4.06 ₄	4.15 ₄	89.9 ₇	90.0 ₀	90.0 ₄	68.6 ₄
P3	4.05 ₆	4.05 ₈	4.15 ₈	89.9 ₆	90.0 ₀	90.0 ₁	68.4 ₂

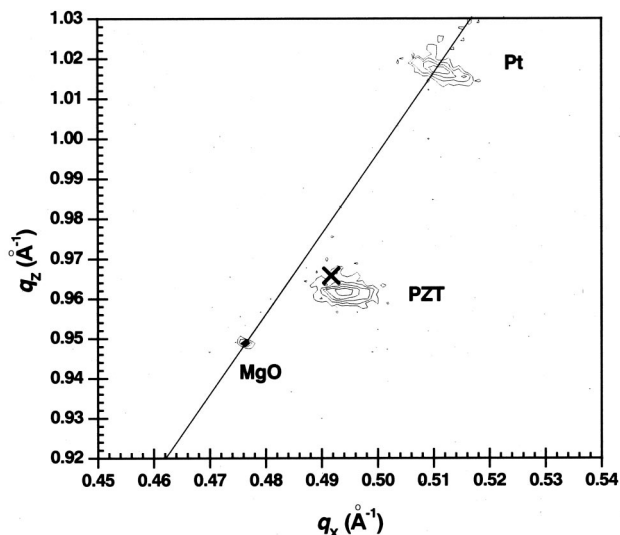


FIG. 3. Reciprocal space map of the PZT/Pt/MgO (P3) heterostructure measured close to their (204) reflections. The × mark shows the PZT (204) peak position of the corresponding powder specimen. The contour interval is logarithmic.

by regarding the structure as a tetragonally crystallized perovskite type. The diffraction patterns contained several limited diffraction peaks for Pt film and residual MgO substrate; however, no peaks were found for impurities such as PbO or pyrochlore.⁷ We assume that the crystal structures of these three PZT specimens were all the same as the tetragonal BaTiO₃ with space group $P4mm$.⁸ Pb (a bivalent positive ion) occupies the 1(a) site (A site), Zr and Ti (tetravalent positive ions) randomly occupy the 1(b) site (B site), and O (a bivalent negative ion) occupies the 1(b) and 2(c) sites (see Fig. 5). The structure of PZT was precisely determined using the Rietveld method,⁹ together with Pt and MgO under conditions where the lattice constant of Pt was fixed at $a = 3.9231 \text{ \AA}$ (Ref. 10) as standard, with those of the other two phases variable. The analytical program used was RIETAN.¹¹ We carried out the Rietveld analyses with the data from 5.0°

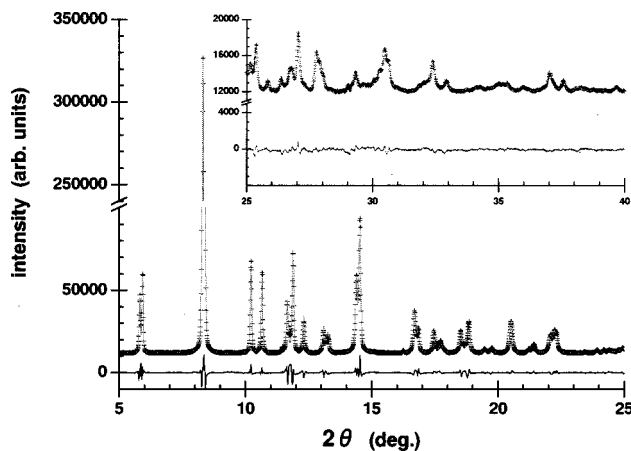


FIG. 4. Observed (+) and calculated (gray line) synchrotron diffraction patterns of $\text{Pb}_{0.97}(\text{Zr}_{0.58}\text{Ti}_{0.45})\text{O}_3$ (P3) at room temperature of 300 K. The difference curve (observed-calculated) appears at the bottom of the figures.

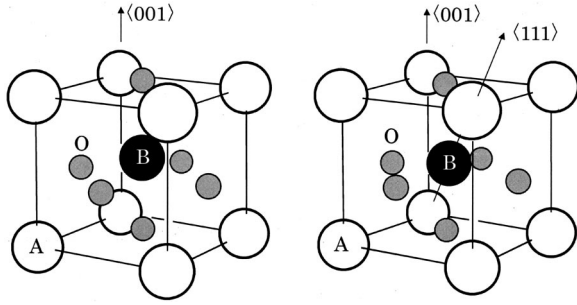


FIG. 5. The tetragonal perovskite crystal structure for $\text{Pb}_{1.15}(\text{Zr}_{0.48}\text{Ti}_{0.37})\text{O}_3$ (P1) is shown schematically in perspective (left). The structure, virtually analyzed as a rhombohedral phase, is on the right.

to 40.0° under the assumption of anisotropic temperature factors for Pb and isotropics for Zr/Ti and O. In addition, the thermal vibrations of O(1) [at the 1(*b*) site] and O(2) [at the 2(*c*) site] were assumed to be identical. Neutral atomic scattering factors were applied to all of the atoms. The results are shown in Fig. 4 and Table IV.

IV. DISCUSSION

A. Thin film on substrate

In this section, we will discuss the film under the restrictions imposed by the substrate. The (204) peak position for the powdered P3 specimen is shown by the “ \times ” mark in Fig. 3. The position was obtained using the lattice constants estimated by means of Rietveld analysis. The relationship in position between the \times mark and the (204) peak of the PZT film indicates that the crystal lattice of the film expands perpendicularly to the substrate surface and is compressed par-

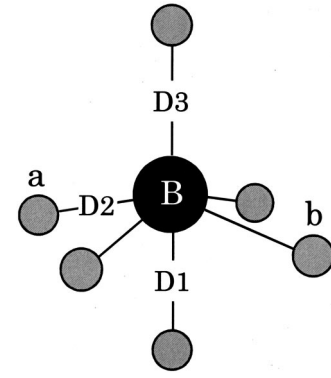


FIG. 6. The coordination geometry around the metal cation (Zr/Ti and Pb) at the *B* site can be described as a distorted oxygen octahedron with three kinds of interatomic distances of D1, D2, and D3.

allel to the surface, compared with that of the powdered specimen. Similar results were obtained for P1 and P2. It can be assumed that little macroscopic stress remains in the powdered specimen. These results indicate that the PZT films experience compressive plane (biaxial) stress parallel to the surface. The stress is isotropic, since *a* coincides closely with *b* as shown in Table III. The PZT film was grown on the Pt (001) square lattice. a_{PZT} is only a little longer than a_{Pt} , which suggests that the PZT (001) plane fell easily in place parallel to the Pt (001) plane. It is assumed that the difference in the lattice spacing between the two ($a_{\text{PZT}} > a_{\text{Pt}}$) generated the compressive stress in the epitaxially grown PZT film.¹² The three films examined in this study were formed in a composition region where rhombohedral crystals are present, as shown in Fig. 1. It is logical, however, to presume that in the isotropic plane stress field, the cations or anions

TABLE IV. Refined structural parameters derived by Rietveld analysis. The space group $P4mm$ was applied to all. Standard deviations are shown in parentheses. $U_{11} = U_{22}$, and $U_{12} = U_{23} = U_{13} = 0$.

P1, $R_{\text{wp}} = 3.19\%$, $R_I = 0.57\%$, $R_e = 0.85\%$, $a = 4.0931(2)$, $c = 4.1235(3)$ Å, $M = \text{Zr}_{0.57} + \text{Ti}_{0.43}$							
Atom	Site	<i>g</i>	<i>x</i>	<i>y</i>	<i>z</i>	U_{11}, U_0 (Å ²)	U_{33} (Å ²)
Pb/ <i>M</i>	1(<i>a</i>)	0.983(9)/0.017	0	0	0	0.034(4)	0.025(7)
Pb/ <i>M</i>	1(<i>b</i>)	0.167/0.833	1/2	1/2	0.556(4)	0.002(4)	
O(1)	1(<i>b</i>)	1.0	1/2	1/2	0.073(37)	0.045(21)	
O(2)	2(<i>c</i>)	1.0	1/2	0	0.429(21)	0.045	
P2, $R_{\text{wp}} = 2.78\%$, $R_I = 0.85\%$, $R_e = 0.84\%$, $a = 4.0830(2)$, $c = 4.1189(2)$ Å, $M = \text{Zr}_{0.58} + \text{Ti}_{0.42}$							
Atom	Site	<i>g</i>	<i>x</i>	<i>y</i>	<i>z</i>	U_{11}, U_0 (Å ²)	U_{33} (Å ²)
Pb/ <i>M</i>	1(<i>a</i>)	0.978(7)/0.022	0	0	0	0.037(3)	0.016(4)
Pb/ <i>M</i>	1(<i>b</i>)	0.089/0.911	1/2	1/2	0.550(4)	0.006(4)	
O(1)	1(<i>b</i>)	1.0	1/2	1/2	0.054(34)	0.056(14)	
O(2)	2(<i>c</i>)	1.0	1/2	0	0.466(26)	0.056	
P3, $R_{\text{wp}} = 3.21\%$, $R_I = 0.87\%$, $R_e = 0.80\%$, $a = 4.0652(2)$, $c = 4.1415(2)$ Å, $M = \text{Zr}_{0.56} + \text{Ti}_{0.44}$							
Atom	Site	<i>g</i>	<i>x</i>	<i>y</i>	<i>z</i>	U_{11}, U_0 (Å ²)	U_{33} (Å ²)
Pb/ <i>M</i>	1(<i>a</i>)	0.921(7)/0.079	0	0	0	0.032(2)	0.017(3)
Pb/ <i>M</i>	1(<i>b</i>)	0.049/0.951	1/2	1/2	0.546(3)	0.010(4)	
O(1)	1(<i>b</i>)	1.0	1/2	1/2	0.079(16)	0.032(11)	
O(2)	2(<i>c</i>)	1.0	1/2	0	0.601(10)	0.032	

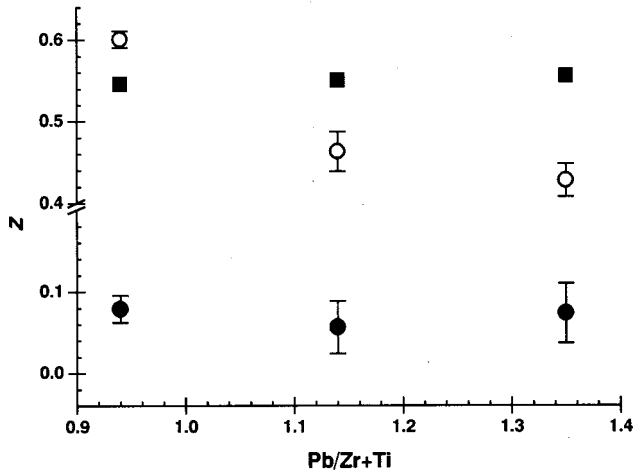


FIG. 7. The atomic positions, z of Zr/Ti (■), O(1) (●) and O(2) (○) are shown as a function of the atomic ratio of Pb/Zr+Ti. The errors for z of Zr/Ti are smaller than the marks.

shift more easily in a $\langle 001 \rangle$ direction perpendicular to the substrate surface than in a $\langle 111 \rangle$ direction. It is therefore concluded that the growth on the Pt (001) plane and the isotropic plane stress are the main factors contributing to the PZT films crystallizing tetragonally and spontaneously polarizing in the c -axis direction.

B. Powder crystal structural analysis

1. Features of the crystal structure

The precise structural analyses using the Rietveld method revealed that all three types of powdered films crystallized into tetragonal perovskite at room temperature. The results of the quantitative analyses for the PZT films showed that the unit cell ought to contain almost exactly two metal atoms. However, the ratio of Pb and Zr+Ti was not 1:1. We then set the following conditions for the Rietveld analyses:

$$g_{\text{Zr/Ti}}^A = 1 - g_{\text{Pb}}^A, \quad g_{\text{Pb}}^B = y - g_{\text{Pb}}^A, \quad \text{and} \quad g_{\text{Zr/Ti}}^B = 1 - g_{\text{Pb}}^B, \quad (1)$$

and conducted the analyses regarding g_{Pb}^A as an independent variable and assuming a partial substitution of Pb atoms at the A site and Zr/Ti atoms at the B site. Here, g_{Pb}^A represents the occupation rate of Pb at the A site, and y represents the number of Pb atoms contained in the unit cell. It was assumed that Zr and Ti atoms were exchanged for Pb while maintaining the composition ratio obtained by quantitative analysis. As shown in Table IV, Pb and Zr/Ti atoms are replaced mutually and partially between the A and B sites in every specimen. In the specimens for which $y > 1$, an excess

TABLE V. Interatomic distances and bond angles. Standard deviations are shown in parentheses.

Specimen	D1 (Å)	D2 (Å)	D3 (Å)	Bond angle (°)
P1	1.990(157)	2.112(21)	2.134(157)	151.3(4.4)
P2	2.045(144)	2.077(17)	2.074(144)	160.6(5.6)
P3	1.934(71)	2.045(5)	2.207(71)	167.2(2.6)

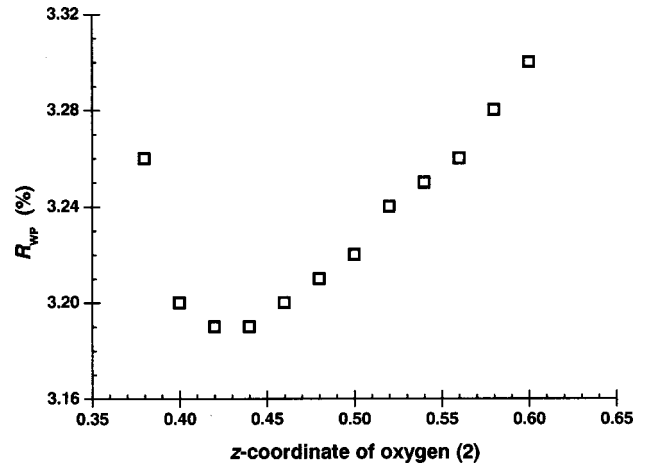


FIG. 8. Agreement factor R_{wp} as a function of O(2) displacement for refinements with fixed values of z along the tetragonal $\langle 001 \rangle$ direction.

of Pb tends to invade the B site and randomly occupy the site together with Zr and Ti. Conversely, in the specimen for which $y < 1$, the excess Zr/Ti atoms tend to mix with Pb at the A site. The O atoms form an octahedron distorted in the c -axis direction surrounding Zr/Ti (see Fig. 6). When PZT is in the high-temperature phase, the cubic perovskite ($Pm\bar{3}m$) phase, Pb, Zr/Ti, O(1), and O(2) are located at $(0,0,0)$, $(\frac{1}{2}, \frac{1}{2}, \frac{1}{2})$, $(\frac{1}{2}, \frac{1}{2}, 0)$, and $(\frac{1}{2}, 0, \frac{1}{2})$, respectively. When P3 ($y < 1$) in the low-temperature phase, all the Zr/Ti, O(1), and O(2) atoms are shifted towards the positive side along the c axis. This shift is expressed as $(+ + +)$ following the notation of Glazer *et al.*¹³ In the cases of P1 and P2 ($y > 1$), however, O(2) shifted towards the negative side, as did $(+ + -)$. The shift of each atom is shown in Fig. 7 as a function of Pb/(Zr+Ti). Although the Zr/Ti and O(1) atom positions change very little in response to Pb/(Zr+Ti), the O(2) atom position shifts significantly. In particular, a large shift towards the negative side was identified for the O(2) atom in the P1 specimen. The coordination number of Zr/Ti atom is six. In this coordination number, the radii of both Pb^{2+} and Pb^{4+} ions are greater than those of Zr^{4+} and Ti^{4+} ions.¹⁴ In

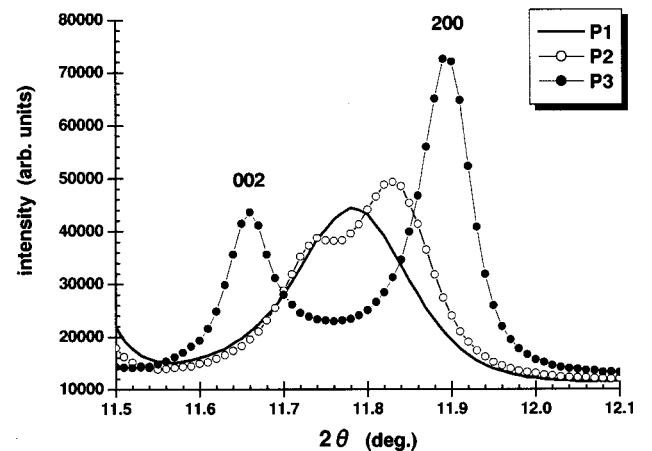


FIG. 9. Diffraction profiles of the (002) and (200) peaks of the PZT powder specimens.

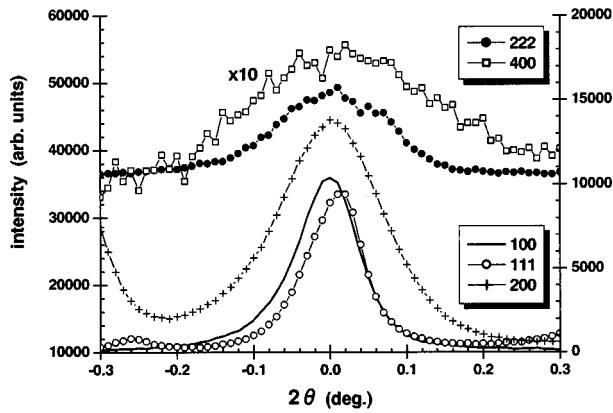


FIG. 10. Diffraction profiles of (100), (111), (200), (222), and (400) of $\text{Pb}_{1.15}(\text{Zr}_{0.48}\text{Ti}_{0.37})\text{O}_3$ (P1) powder specimen. The former three are shown on the left scale and the latter two on the right. (400) is multiplied by 10.

P1, Pb occupies no less than about 17 at.% of the B site, which means the ionic radius at this site is significantly larger than in the case of P3. It is assumed that the $\text{O}(2)$ atoms shift towards the negative side as a result of being physically pushed by the atoms at the B sites. At the same time, the interatomic distance between $\text{Zr}/\text{Ti}-\text{O}(2)$ (a - B) extended with increased presence of Pb, and the bond angle of $\text{O}(2)-\text{Zr}/\text{Ti}-\text{O}(2)$ (a - B - b) becomes smaller (see Fig. 6 and Table V). To confirm the correctness of the determined z value of $\text{O}(2)$, we performed Rietveld analyses for P1 under conditions where the atomic position of $\text{O}(2)$ was fixed and the other parameters were variable. The results are shown in Fig. 8. As shown in this figure, R_{wp} has a minimum value of around $z = 0.43$.

2. Deformation of crystal structure depending on composition

As shown in Fig. 9, the tetragonal (200) and (002) peaks are clearly separated for P3. With increased $\text{Pb}/(\text{Zr} + \text{Ti})$, however, c/a approaches unity and the two peaks coalesce. In particular, it is difficult in P1 to distinguish whether there is a single peak, indicating a rhombohedral crystal, or whether there are two overlapping peaks indicating a tetragonal crystal. Figure 10 shows the profiles for (100), (111), (200), (222), and (400) diffraction peaks obtained for P1. A rhombohedral crystal should show two peaks, (111) and $(\bar{1}\bar{1}1)$, and should show (222) and $(\bar{2}\bar{2}2)$ in its powder diffraction profile; however, no such peak split can be seen in Fig. 10. As shown in Table VI, in these five peaks, the correspondence between singlet/doublet and tetragonal/

TABLE VI. Independent reflections in rhombohedral and tetragonal structures and the FWHM's estimated from the observed peaks of $\text{Pb}_{1.15}(\text{Zr}_{0.48}\text{Ti}_{0.37})\text{O}_3$ (P1). The peak positions are shown in the 2θ column.

Rhomb.	Tetra.	FWHM ($^\circ$)	2θ ($^\circ$)
100	001, 100	0.097	5.88
111, $\bar{1}\bar{1}1$	111	0.088	10.18
200	002, 200	0.162	11.77
222, $\bar{2}\bar{2}2$	222	0.189	20.45
400	004, 400	0.288	23.66

rhombohedral becomes completely inverted. The full width at half maximum (FWHM) of each diffraction peak was estimated by fitting a pseudo-Voigt function using the least-squares method. These results are also shown in Table VI. No matter what crystal system the specimen belongs to, FWHM tends to spread more in doublets than in singlets. As seen in the table, it is logical to conclude, from the disposition in the FWHM's in the diffraction peaks, that P1 crystallizes into a tetragonal system.

The tetragonal PZT belongs to the space group $P4mm$ (C_{4v}^1); on the other hand, the rhombohedral PZT belongs to the space group $R3m$ (C_{3v}^5) at room temperature. None of these is a subgroup of the symmetry of the other.¹⁵ This suggests that the phase transition of this compound depending on the composition is a first-order phase transition. In that case, two phases can co-exist.¹⁶ In fact, Kakegawa *et al.*¹⁷ have reported that these two phases co-exist around MPB on the PbTiO_3 - PbZrO_3 pseudobinary system. This suggests that a small amount of the rhombohedral phase may also co-exist in our specimens, especially in P1, while most or all of P1 crystallizes in the tetragonal phase as mentioned above.

We then attempted a Rietveld analysis under the assumption that P1 has a rhombohedral structure. The structural model followed the description of Glazer *et al.*¹⁸ in which Pb, Zr/Ti, and O atoms occupy $1(a)$, another $1(a)$, and $3(b)$ sites in the space group $R3m$, respectively. Pb was fixed at 0,0,0. The results obtained are shown in Table VII, and the crystal structure is illustrated in Fig. 5. The final R factors showed fairly good values. As can be seen in this figure, the rhombohedral structure is almost the same as the tetragonal structure. This means at least that P1 can be approximately described using a rhombohedral structure; it also suggests that the transition from one phase to the other can be enabled by slight shifts in atomic position.

TABLE VII. Refined structural parameters obtained by Rietveld analysis. The space group $R3m$ was applied. Standard deviations are shown in parentheses. $U_{11} = U_{22} = U_{33}$ and $U_{12} = U_{23} = U_{13}$.

P1, $R_{\text{wp}} = 3.26\%$, $R_I = 0.75\%$, $R_e = 0.85\%$, $a = 4.1020(2)$ Å, $\alpha = 89.862(10)^\circ$, $M = \text{Zr}_{0.57} + \text{Ti}_{0.43}$							
Atom	Site	g	x	y	z	U_{11}, U_0 (\AA^2)	U_{12} (\AA^2)
Pb/M	$1(a)$	0.992(11)/0.008	0	0	0	0.033(4)	-0.014(5)
Pb/M	$1(a)$	0.158/0.842	0.527(5)	0.527	0.527	0.003(7)	
O	$3(b)$	1.0	0.448(15)	0.448	0.038(51)	0.046(31)	

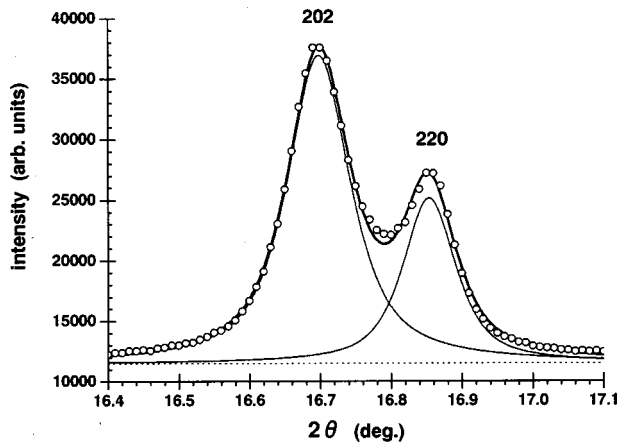


FIG. 11. Diffraction profile of the (202) and (220) peaks of the $\text{Pb}_{0.97}(\text{Zr}_{0.58}\text{Ti}_{0.43})\text{O}_3$ (P3) powder specimen. The open circles show the observed intensity. The thin lines are the symmetrical pseudo-Voigt functions fitted by the least-squares method. The thick line is the synthetic curve of the two.

The present PZT films on the Pt (001) plane are tetragonal perovskites. If the films were grown on a Pt (111) plane, some or all of them might crystallize in the rhombohedral phase. Further investigations are required. Moreover, the above results and discussions suggest that, also, y in $\text{Pb}_y(\text{Zr}_{0.57}\text{Ti}_{0.43})_{2-y}\text{O}_3$ can be a factor affecting the phase transition from the tetragonal system to the rhombohedral system, like x in $\text{Pb}(\text{Zr}_x\text{Ti}_{1-x})\text{O}_3$. We also wish to continue our studies on crystal structure with $\text{Pb}/(\text{Ti}+\text{Zr})$ as a parameter.

As described in the Introduction, in bulk PZT ceramics, the existence of a monoclinic structure has been revealed to be a low-temperature variant of the tetragonal phase in the composition region near MPB. This monoclinic phase also exists at room temperature depending on composition. Figure 11 shows the (202) and (220) diffraction peaks obtained for P3. If it were a monoclinic crystal (m), four peaks, $(22\bar{2})_m$, $(222)_m$, $(400)_m$, and $(040)_m$ should be observed. However, the obtained diffraction profile could be described almost perfectly as the sum of two symmetrical pseudo-Voigt functions, leading to the conclusion that the diffraction profile seen in Fig. 11 consists of only the (202) and (220) peaks of the tetragonal structure. As mentioned above, the films were grown on the Pt (001) lattice plane with a fourfold rotation axis perpendicular to the plane surface. Since the rhombohedral crystal does not grow on it, it is unlikely that a monoclinic crystal without fourfold rotation symmetry would grow.

V. CONCLUSIONS

All of the thin films of $\text{Pb}_y(\text{Zr}_{0.57}\text{Ti}_{0.43})_{2-y}\text{O}_3$ ($y = 0.97, 1.07, 1.15$) formed on a Pt(001)/MgO(001) substrate using the rf sputtering method were grown epitaxially with the “cube on cube” relationship and crystallized into tetragonal perovskite type structures at room temperature, whereas each of their compositions is in an area where rhombohedral crystals appear, i.e., on the Zr-rich side of the MPB. No other crystalline phases were observed in the films. In the space group $P4mm$, the Pb atoms occupy the A ($1a$) site, and the Zr and Ti atoms occupy the B ($1b$) site at random. The O atoms occupy the O ($1b+2c$) site and form an octahedron that is distorted along the c -axis direction surrounding Zr/Ti. For every specimen, Pb and Zr/Ti are partially substituted for each other. When Zr/Ti is greater than Pb ($y < 1$), the excess Zr/Ti atoms tend to invade the A site; on the other hand, when Pb is greater than Zr/Ti ($y > 1$), the excess Pb atoms tend to invade the B site. For any specimen, the atomic positions of Zr/Ti and O are shifted from the equilibrium atomic positions in the paraelectric phase, resulting in spontaneous polarization. Although the Zr/Ti and O ($1b$) atomic positions change very little in response to Pb/Zr+Ti, the O ($2c$) position shifts significantly. All of the specimens are in the tetragonal phase; however, with increased of Pb/(Zr+Ti), the crystal structure approaches the rhombohedral phase. The PZT film grows on the Pt (001) square lattice and an isotropic compressive plane stress is present in the film. These are the major factors that cause the PZT film to be crystallized tetragonally and polarize it along the direction of not a diagonal axis, but the c axis. These PZT films remained frozen in tetragonal form when powdered and released from the stress. No phase transition to any other crystal structure was observed.

ACKNOWLEDGMENTS

The authors would like to express their thanks to Mr. K. Katoh at the Japan Synchrotron Radiation Research Institute, to Dr. Y. Kubota at the Department of Environmental Sciences, Faculty of Science, Osaka Women’s University, and Dr. E. Nishibori, Assistant Professor M. Takata and Professor M. Sakata at the Department of Applied Physics at Nagoya University, for their great assistance in the experiments at BL02B2 and their advice on structural analyses. They also wish to thank Professor K. Wasa of the Department of Environment Science Faculty of Science at Yokohama City University for his valuable suggestions concerning this study.

¹B. Jaffe, W. R. Cook, and H. Jaffe, *Piezoelectric Ceramics* (Academic, London, 1971).

²B. Noheda, A. Gonzalo, L. E. Cross, R. Guo, S. E. Park, D. E. Cox, and G. Shirane, *Phys. Rev. B* **61**, 8687 (2000).

³K. Wasa, Japan Society for the Promotion of Science, Elastic Wave Element Technology No. 150 Committee, 72nd Workshop, Materials (2001) (in Japanese).

⁴*Experimental Chemistry Lectures*, edited by the Chemical Society of Japan (Maruzen, Tokyo, 1992) (in Japanese).

⁵M. Takata and M. Yamakata, *SPring-8 Information* **5** (2), 88 (2000).

⁶M. Sakata, M. Takata, and E. Nishibori, *SPring-8 Information* **5** (3), 194 (2000).

⁷Z. Wang, K. Kikuchi, and R. Maeda, *Jpn. J. Appl. Phys.*, Part 1

- 39**, 5413 (2000).
- ⁸*International Tables for Crystallography*, edited by T. Hahn (Kluwer, Dordrecht, 1995), Vol. A.
- ⁹H. M. Rietveld, *J. Appl. Crystallogr.* **2**, 65 (1969).
- ¹⁰R. W. G. Wyckoff, *Crystal Structures*, Vol. 1 (Interscience, New York, 1963).
- ¹¹F. Izumi, *J. Crystallogr. Soc. Jpn.* **27**, 23 (1985) (in Japanese).
- ¹²K. Abe, S. Komatsu, N. Yanase, K. Sato, and T. Kawakubo, *Jpn. J. Appl. Phys., Part 1* **36**, 5846 (1997).
- ¹³A. M. Glazer and S. A. Mabud, *Acta Crystallogr., Sect. B: Struct. Crystallogr. Cryst. Chem.* **B34**, 1065 (1978).
- ¹⁴A. R. West, *Basic Solid State Chemistry* (John Wiley & Sons, Chichester, 1984).
- ¹⁵B. K. Vainshtein, V. M. Fridkin, and V. L. Indenbom, *Structure of Crystals* (Springer-Verlag, Berlin, 1995).
- ¹⁶L. D. Landau, A. I. Akhiezer, and E. M. Lifshits, *General Physics* (Pergamon, Oxford, 1967).
- ¹⁷K. Kakegawa, J. Mohri, S. Shirasaki, and K. Takahashi, *J. Am. Ceram. Soc.* **65**, 515 (1982).
- ¹⁸A. M. Glazer, S. A. Mabud, and R. Clarke, *Acta Crystallogr., Sect. B: Struct. Crystallogr. Cryst. Chem.* **B34**, 1060 (1978).